Dynamic deformation of Metastable Austenitic Stainless Steels at the nanometric length scale

J.J. Roa[1,2,*], I. Sapezanskaia[1,2,3], G. Fargas[1,2], R. Kouitat[2], A. Redjaïmia[2], A. Mateo[1,2]

[1] CIEFMA-Dept. of Materials Science and Engineering, Universitat Politècnica de Catalunya, EEBE-Campus Diagonal Besòs, 08019 Barcelona, Spain

[2] Centre for Research in NanoEngineering, Universitat Politècnica de Catalunya, EEBE-Campus Diagonal Besòs, 08019 Barcelona, Spain

[3] Institut Jean Lamour, UMR 7198 CNRS, Université de Lorraine, 54840 Nancy Cedex, France

[*] Corresponding author, e-mail: joan.josep.roa@upc.edu

Abstract: Cyclic indentation was used to evaluate the dynamic deformation on metastable steels, particularly in an austenitic stainless steel, AISI 301LN. In this work, cyclic nanoindentation experiments were carried out and the obtained loading-unloading (or P-h) curves were analyzed in order to get a deeper knowledge on the time-dependent behavior, as well as the main deformation mechanisms. It was found that the cyclic P-h curves present a softening effect due to several repeatable features (pop-in events, ratcheting effect, *etc.*) mainly related to dynamic deformation. Also, observation by transmission electron microscopy highlighted that dislocation pile-up is the main responsible of the secondary pop-ins produced after certain cycles.

Keywords: metastable stainless steels, cyclic nanoindentation tests, transmission electron microscopy, time-dependent, plastic deformation, ratcheting effect.

1. Introduction

During the last decade, TRansformation Induced Plasticity (TRIP) steels have received special attention in the automotive industry due to their interesting features as manufacturability, crashworthiness and feasibility for weight reduction [1,2,3]. In the particular case of metastable austenitic stainless steels, plastic deformation can induce phase transformation (from austenite into martensite, $\gamma \rightarrow \alpha'$). Those steels have a high ductility and remarkable fatigue response, as reported in Refs. [4,5].

Some macroscopic experiments have been conducted to identify the influence of the different plastic deformation mechanisms, in particular the phase transformation, on the fatigue behavior of TRIP steels [6,7,8,9,10,11]. This mechanism is the main responsible to generate a hardening behavior on TRIP steels, which is in fair agreement with the data reported by Roa *et al.* [12]. On the other hand, at the micro- and nanometric length scale, the behavior of austenitic TRIP steels under cyclic indentation may be quite different from that at the macroscopic length. At small scale, the effect of heterogeneities (*i.e.,* austenitic grains with different crystallographic orientations, grain boundaries, martensitic lamella, inclusions, among others) on cyclic indentation response is not completely well understood. One of the important characteristics in plastic deformation of metallic materials subjected to cyclic mechanical loading is the change of the deformation resistance with the loading cycles, as was reported by Yang *et al.* [13]. Furthermore, most metals display a dependence of hardening and/or softening with the loading cycles [13], which indicates that these phenomena may be related to the nucleation and propagation of dislocations, as well as to the initiation and accumulation of damage. On the other hand, at the submicrometric length scale, the unloading process can no longer be considered simple elastic deformation recovery as in homogeneous material [14], acting the cyclic indentation response as an indicator for the possible inelastic behavior.

Within this context, the main purpose of this study is to understand the mechanical and microstructural behavior of TRIP steels under cyclic indentation. In doing so, advanced characterization techniques (nanoindentation, EBSD, OIM and TEM) were used to observe and to characterize the main deformation mechanisms induced under cyclic complex stress field.

2. Experimental procedure

2.1 Material

Samples of commercial AISI 301LN stainless steel (equivalent to EN 1.4318) were supplied as 1.5 mm thick sheets by Outokumpu (Finland). After annealing at 1100 ºC for 1 h, the steel presented a fully homogeneous austenitic microstructure. The chemical composition for the material of study is given in **Table 1**.

Prior to the micromechanical and microstructural characterization, specimens were polished using diamond suspensions with gradually decreasing particle sizes from 30 to 1 μm. After mechanical polishing, the specimens were electrochemically polished at room temperature using a constant voltage of 23 V in order to remove the work hardened layer induced during the previous polishing process.

2.2. Micromechanical properties: cyclic tests

The cyclic tests were performed at the micrometric length scale by using the nanoindentation technique, with an ultra-nanohardness tester (UNHT) from CSM instruments. A Berkovich tip indenter was used whose the shape of the latter was carefully calibrated for true indentation depth as small as 20 nm by indenting fused silica samples of known Young's modulus (72 GPa).

Cyclic indentations (2, 10 and 50 cycles) were performed in different austenitic grains to investigate the main plastic deformation mechanisms and also the local mechanical response at the micrometric length scale within the austenitic grains in order to avoid any grain boundary (GB) effect. Furthermore, the loading and unloading rates were held constant and equals to 15 $mN \cdot min^{-1}$ for all the tests. **Table 2** summarizes the main parameters employed to perform the cyclic indentation test.

2.3. Crystallographic and deformation mechanisms characterization

Crystal orientation in the region where the micromechanical properties were evaluated was assessed by means of Electron BackScattered Diffraction (EBSD). It was conducted in a Field Emission Scanning Electron Microscope (FESEM) JEOL 7001F equipped with an Orientation Imaging Microscopy (OIM) system. The diffraction response of grains oriented with a surface normal near the basal direction was sufficient for indexing with a beam current of 1 nA.

EBSD measurements were performed with a constant scanning step of 100 nm at an acceleration voltage of 20 kV.

Transmission Electron Microscopy (TEM) was employed for detailed study of the deformation mechanisms associated with the plastic deformation induced during the cyclic indentation process. Hence, TEM lamellae were directly extracted by Focused Ion Beam (FIB) using a dual beam Workstation (Zeiss Neon 40). In doing so, prior to milling a thin platinum layer was deposited on residual imprints to be studied. A Ga^+ source was used, and current and acceleration voltage were progressively decreased to a final polishing stage of 10 pA. Deformation features within the FIB-milled lamellae were examined in a TEM equipment (Philips CM200) operating at 200 kV.

3. Results and discussion

3.1. Loading-unloading curves: time dependence effect

Figure 1 displays the two loading-unloading (P-h) curves at a maximum applied load of 6 mN. The difference between them is that in the first case (Fig. 1a) unloading begins immediately after reaching the maximum load (i.e. holding time is zero), whereas in the second one (Fig. 1b) the indenter reaches the maximum applied load and keeps it constant for 10 s. In both cases, P-h curves clearly do not overlap. This observation highlights that the cyclic indentation process is not ideally reversible, producing a permanent deformation. Furthermore, for the curves without holding time (**Figure 1a**), the indenter continues moving into the material in a similar way to creep deformation. However, at difference from the creep flow, in the present case this is likely related to the time-dependent behavior, also known as dynamic behavior. This observation is in fair agreement with the results reported for metastable stainless steels in Refs. [15,16,17,18]. As shown in both figures (**Figures 1a** and **1b**), each hysteresis loop represents a maximum and minimum deformation located in the center of the loop. Furthermore, the open hysteresis loops can be described as a consequence of increasing dislocation density. As cyclic loading-unloading cycle is asymmetric in nature, certain number of dislocations generated during forward loading do not get annihilated during backward loading sequence, remaining thus significant amount of dislocations in the sub-structure which cause the increase in dislocation density [19]. This phenomenon, also known as ratcheting strain accumulation effect, has been previously observed for austenitic stainless steels under conventional fatigue testing, as reported elsewhere [15,17,20,21,22,23]. Misra *et al.* [24] found the same trend described above at the local scale by using the nanoindentation technique for austenitic grains, whereas the loops for the martensite phase were close. This difference may be related with the different crystallographic structure of both phases, being dislocations more mobile in austenite than in martensite. Thus, the cyclic indentation process highlights the ratcheting behavior of metastable stainless steels, which is strongly correlated with the dislocation activity.

Under loading control mode indentation was conducted for 50 cycles, between 50 and 100% of the peak load, as it is depicted in **Figure 2a.** In this figure, pop-ins labelled as (1) and (2) appear in the loading curve and during the holding time, respectively. These discontinuities represent an abrupt increase in the penetration depth on a nanoindentation curve. The first pop-in appears at less than 50 μN of applied load, and it may be attributed to the transition from elastic-to-plastic deformation. The fitting of the experimental points by using the Hertz equation, $P \approx C \cdot h^{3/2}$ [25,26,27], confirms that this discontinuity in the loading curve marks the conversion from elasticity to plasticity. After this applied load, a plastic deformation will appear. Furthermore, the elastic nature of the unloading/reloading response is clearly evident. This phenomenon may be related to the different plastic deformation mechanisms activated under these loading conditions, which produce a permanent deformation. Also, **Figure 2a** exhibits a drift toward large displacement starting from the first loading cycle, which may be related to the time-dependent behavior as frequently observed in metallic materials under indentation. This is in perfect agreement with the trend observed for bulk Al specimen [28].

Figure 2b exhibits the applied load (*P*) and the penetration depth (*h*) as a function of the time (*t*) for ten cycles. The loading curve versus time (*P*-*t*) was conducted between 10% and 100% of the peak load, working under loading control mode. On the other hand, the penetration depth against the time (*h*-*t*), presents a softening mechanisms after the fourth cycle. Initially, the penetration depth was held constant and around 13 nm, while after this cycle the penetration depth abruptly increases until reach a value ranged between 15-16 nm. This phenomenon may be related to the strain accumulation during the cyclic process. In this regard, after the fourth cycle the strain generated is enough to increase considerable the dislocation activity under the residual imprint. Furthermore, during the holding time in the *h-t* curve, it exists a considerable fluctuation, which may be is related with the activation of the dislocation activity induced by the strain produced during the holding segment.

Figure 3a exhibits the cyclic indentation P-h curves for 50 cycles, which were conducted between 1% and 100% of the peak working under loading control mode. In this representation, each cycle is shifted 10 nm in order to clearly observe the cycle shape. It is evident that a stress relaxation or softening mechanisms takes places after the first indentation cycle. This effect may be related to the ratcheting phenomena discussed in **Figure 1** or, as suggested by Li and Chu [29], negative dislocations are likely emitted from the contact edge between the indenter and the specimen, which reduce the dislocation density underneath the indenter and cause local softening and reverse plastic flow.

In **Figure 3b**, six different cycles are presented in order to observe the real shape, which highlights that the same deformation features, as explained in **Figure 1,** occur, *i.e.,* progressive open loops toward deeper penetrations over the cycles. Furthermore, in this particular case, the inelastic nature of the unloading/reloading response is obvious, and the deformation did not reach stabilization after 50 cycles.

Apart of the softening effect observed after certain cyclic tests (labelled as * in **Figure 4**), it can be clearly seem that several pop-ins appear in the loading curve as well as in the holding segment; marked with a dash circle and labelled as (1) and (2), respectively, after several indentation cycles. This phenomenon is often associated to the first stage of plastic deformation, mainly related to dislocation motion, when it takes place during the first loading curve, which is not the case. Furthermore, the shape of the individual cyclic curves is similar to those reported in **Figure 1** and **3**.

It is well stablished [30,31,32,33,34] that the nanoindentation tests in metallic materials near the GB leads to the activation of secondary pop-ins at applied loads higher than those producing the elastic-to-plastic transition. These pop-ins present a variable width, ranged between 10 to 100 nm, and may be related to dislocation pile-up at the GB and subsequent slip transfer across it, as reported in Refs. [37,35]. In this regard, Wang and Ngan [30] deduced that this phenomenon occurs at a critical *c/d* value, where *c* is the size of the plastic zone and *d* is the distance from the center of the residual imprint to the GB.

3.2. Plastic deformation mechanisms

It is well known that for metallic materials under cyclic indentation, the accumulated strain increases the plastic zone size and propagates into the adjacent grains, as reported elsewhere [13,36]. However, scarce information is available when the plastic deformation has been induced under cyclic indentation inside individual austenitic metastable grains.

Attempting to get a more detailed knowledge of the deformation scenario induced by cyclic indentation process at the micrometric length scale, TEM lamellae were extracted by FIB directly from the center of the residual imprint, see **Figure 5**. A general TEM observation of the plastic deformation induced after 15 loading-unloading cycles is presented in **Figure 5a**, where the austenitic grain exhibits a highly-deformed substructure, which expands around the residual imprint and along and through the GB as previously was reported by Sapezanskaia *et al.* [37]. Furthermore, different deformation features activated due to the accumulated strain can be clearly observed: extensive residual stresses beneath the imprint, and dislocation slip rather localized below indentations. On the other hand, due to the accumulation of plasticity in the region in contact with the indenter, the plastic deformation transfers from the indented grain into the adjacent grain when the imprint is performed at the vicinity of a GB, as it is clearly seen in the bright field BF-TEM image, see **Figure 5b**. This phenomenon may be related to the presence of secondary pop-ins, where the dislocation pile-up is the main responsible to produce this effect after certain cycles, as reported in Refs. [30-34].

Furthermore, in the magnified region, a dense dislocation forest is clearly evident at the vicinity of the GB. This deformation can be associated with Shockley partials gliding on successive {111} planes [38]. Also, as reported Roa *et al.* [39], when the imprint is performed near the GB, the austenite grain in contact with the indenter may be subjected to intergranular shearing, being this phenomenon the main responsible to induce phase transformation, from γ to α'-martensitic phase transformation.

5. Conclusions

In this study, cyclic indentation tests were performed in austenitic grains in order to examine the dynamic deformation as well as to evaluate the main deformation mechanisms. The following conclusions can be drawn:

(i) Dynamic deformation points out that metastable stainless steels present an inelastic nature of the unloading/reloading response, which is mainly related to ratcheting effect.

(ii) Cyclic indentation induces a softening effect which is mainly related to the dynamic deformation of metastable stainless steels.

(iii) Dislocation pile-up near the grain boundary is the main responsible to produce secondary pop-ins after certain indentation cycles.

(iv) The predominant deformation mechanism induced under cyclic indentation is the forest dislocation at the GB. Furthermore, due to the strain accumulation the plastic zone increases and propagates the deformation into the neighboring grain.

Acknowledgements

Dr. I. Sapezanskaia would like to thank DOCMASE program for its financial support and J. Säynäjäkangas and A. Kalapudas, from Tornio Research Center Outokumpu (Finland), for providing the steel samples. This work was financially supported by the Spanish Ministerio de Economía y Competitividad (Grant MAT2015-70780-C4-3-P).

References

[1] K. Spencer, J. D. Embury, K. T. Conlon, M. Véron and Y. Bréchet: *Mater. Sci. Eng. A*, 2004, vol. 387-389, pp. 873-881.

[2] Y. H. Kim, K. Y. Kim and Y. D. Lee: *Mater. Manuf. Process.*, 2004, vol. 19**,** pp. 51-59.

[3] K. H. Lo, C. H. Shek and J. K. L. Lai: *Mater. Sci. Eng. R*: 2009, vol. 65, pp. 39-104.

[4] Z. G. Hu, P. Zhu and M. Jin: *Mater. Design*: 2010, vol. 31, pp. 2884-2890.

[5] A. S. Hamada, L. P. Karjalainen, P. K. C. V. Surya and R. D. K. Misra: *Mater. Sci. Eng. A*, 2011, vol. 528, pp. 3890-3896.

[6] G. R. Chanani and S. D. Antolovich: *Metall. Trans.*, 1974, vol. 5, pp. 217-229.

[7] T. B. Hilditch, I. B. Timokhina, L. T. Robertson, E. V. Pereloma and P. D. Hodgson: *Metall. Mater. Trans. A*, 2009, vol. 40**,** pp. 342-353.
[8] L. T. Robertson, T. B. Hilditch and P. D. Hodgson: *Int. J. Fatigue*, 2008, vol. 30, pp. 587-594.
[9] K. I. Sugimoto, M. Kobayashi and S. I. Yasuki: *Metall. Mater. Trans. A*, 1997, vol. 28, pp. 2637-2644.
[10] K. I. Sugimoto, S. M. Song, K. Inoue, M. Kobayashi and S. Masuda: *J. Soc. Mater. Sci.*, 2001, vol. 50, pp. 657-664.
[11] T. Nebel and D. Eifler: *Sadhana-Acad. Proc.Eng. Sci.*, 2003, vol. 28, pp. 187-208.
[12] J. J. Roa, G. Fargas, E. Jiménez-Piqué and A. Mateo: *Mat. Sci. Eng. A*, 2014, vol. 597, pp. 232-236.
[13] F. Yang, L. Peng and K. Okazaki: *J. Mater. Sci.*, 2007, vol. 42, pp. 4513-4520.
[14] W. C. Oliver and G. M. Pharr: J. Mater. Res., 1992, vol. 7, pp. 1564-1583.
[15] F. Yoshida: *Int. J. Press. Vessel. Pip.*, 1990, vol. 44, pp. 207-223.
[16] E. Krempl: *J. Mech. Phys. Solids*, 1979, vol. 27, pp. 363-375.
[17] N. Ohno and M. Abdel-Karim: *J. Eng. Mater. Technol.*, 2000, vol. 122, pp. 35-41.
[18] G. Kang, N. Ohno and A. Nebu: *Int. J. Plast.*, 2003, vol. 19, pp. 1801-1819.
[19] K. Dutta, S. Sivapradad, S. Tarfder and K. K. Ray: *Mater. Sci. Eng. A*, 2010, vol. 527, pp. 7571-7579.
[20] D. Kujawski, V. Kallianpur and E. Krempl: *J. Mech. Phys. Solids*, 1980, vol. 28, pp. 129-148.
[21] E. Krempl and M. B. Ruggles: *J. Mech. Phys. Solids*, 1990, vol. 38, pp. 587-597.
[22] M. B. Ruggles and E. Krempl: *J. Eng. Mater. Technol.*, 1989, vol. 111, pp. 378-383.
[23] J. R. Ellis, D. N. Robinson and C. E. Pugh: *J. Eng. Mater. Technol.*, 1983, vol. 105, pp. 250-256.
[24] R. D. K. Mirsa, P. Venkatsurya, K. M. Wu and L. P. Karjalainen: *Mater. Sci. Eng. A*, 2013, vol. 560, pp. 693-699.

[25] A. C. Fisher-Cripps, Nanoindentation, 2nd ed. New York, United States of America: Springer-Verlag Press; 2004, 3, 9-10.

[26] E. Jiménez-Piqué, Y. Gaillard, M. Anglada: *Key Eng. Mater.*, 2007, vol. 333, pp. 107-116.

[27] J. J. Roa, E. Jiménez-Piqué, X. G. Capdevila and M. Segarra: *J. Eur. Ceram. Soc.*, 2010, vol. 30, pp. 1477-1482.

[28] J. Mueller, K. Durst, D. Amberger and M. Goken: *Mater. Sci. Forum*, 2006, vol. 503-504, pp. 31-36.

[29] J. C. M. Li and S. N. G. Chu : *Scripta Mater.*, 1979, vol. 13, pp. 1021-1026

[30] M. G. Wang and A. H. W. Ngan: *J. Mater. Res.*, 2004, vol. 19, pp. 2478-2486.

[31] T. Ohmura, K. Tsuzaki and F. X. Yin: Steel, *Mater. Trans.*, 2005, vol. 46, pp. 2026-2029.

[32] T. B. Britton, D. Randman and A. J. Wilkinson: *J. Mater. Res.*, 2009, vol. 24, pp. 607-615.

[33] T. Ohmura and K. Tsuzaki: *J. Mater. Res.*, 2007, vol. 42, pp. 1728-1732.

[34] B. Yang and H. Vehoff: *Acta Mater.*, 2007, vol. 55, pp. 849-856.

[35] S. Tsurekawa, Y. Chihara, K. Tashima, S. Li and P. Lejcek: *J. Mater. Sci.*, 2014, vol. 49, pp. 4698-4704.

[36] J. C. M. Li and S. N. G. Chu : *Scr. Metall.*, 1979, vol. 13, pp. 1021-1026.

[37] I. Sapezanskaia, J. J. Roa, G. Fargas, M. Turon-Viñas, T. Trifonov, R. Kouitat Njiva, A. Redjaïmia and A. Mateo: *Mat. Charact.*, 2017, vol. 131, pp. 253-260.

[38] P. J. Ferreira, J. B. Vander Sande, A. Fortes and A. Kyrolainen: *Metall. Mater. Trans. A*, 2004, vol. 35, pp. 3091-3101.

[39] J. J. Roa, J. M. Wheeler, T. Trifonov, G. Fargas, A. Mateo, J. Michler and E. Jiménez-Piqué: *Mat. Sci. Eng. A*, 2015, vol. 647, pp. 51-57.

Figure captions

Figure 1. Magnification at the maximum applied load of cyclic indentation loading-unloading curves with different holding times. (a) 0 s and (b) 10 s.

Figure 2. (a) Loading-unloading curve for all the cyclic tests performed at a maximum applied load of 100 μN and unloaded until half of the maximum applied load and **(b)** Applied load (green curve) and indentation depth (blue curve) as a function of time for an indentation load with the mean load of 75 μN and the indentation frequency of 0.025 cycles/s.

Figure 3. Cyclic evolution of the P-h curves for 50 cycles performed under loading control mode at a maximum displacement into surface of around 5 mN. (a) General view of all cycles, and (b) Detailed view of every tenth cycle. Between each cycle the penetration depth has been shifted 10 nm in order to clearly show the shape of the P-h cycle.

Figure 4. Cyclic P-h evolution where several pop-ins (black dash circles) as well as a softening behavior (labelled as *) can clearly be appreciated.

Figure 5. TEM images corresponding to the central cross section of a residual imprint after 15 loading-unloading nanoindentation cycles. (a) General view of the deformation substructure. The position of the cyclic indentation site is schematically indicated and (b) Magnified bright field (BF) TEM image of the region delimited with a red square. The dash line denotes the GB.

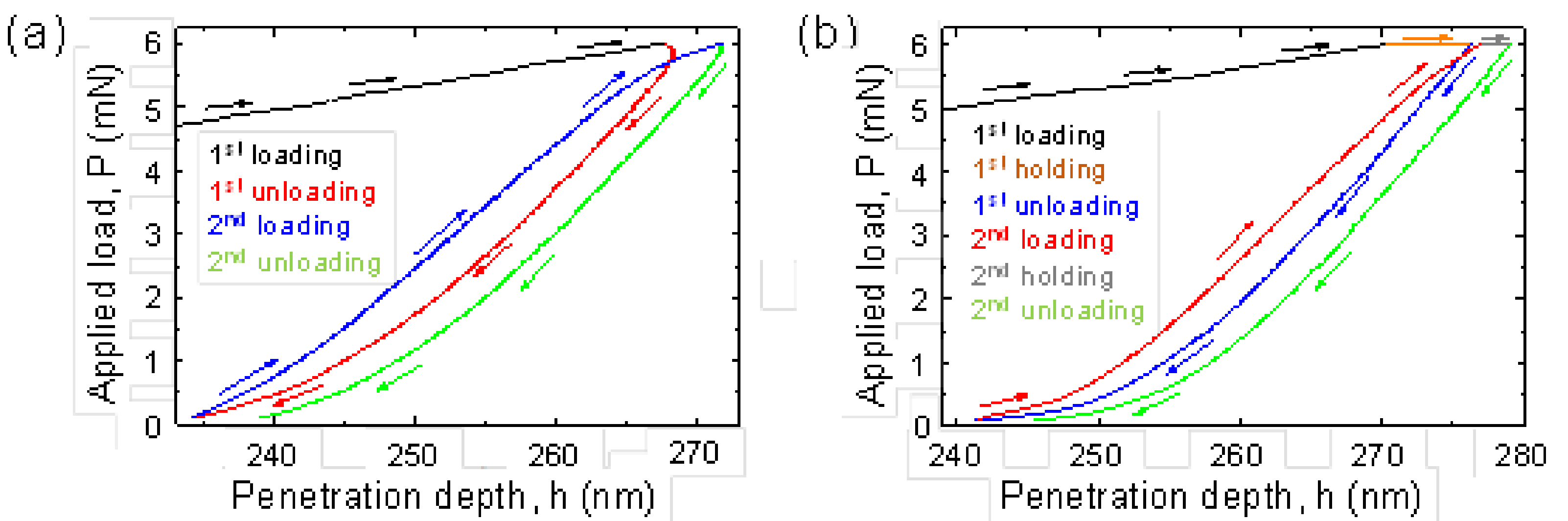
(a)
Applied load, P (mN)
Penetration depth, h (nm)
1st loading
1st unloading
2nd loading
2nd unloading
(b)
Applied load, P (mN)
Penetration depth, h (nm)
1st loading
1st holding
1st unloading
2nd loading
2nd holding
2nd unloading

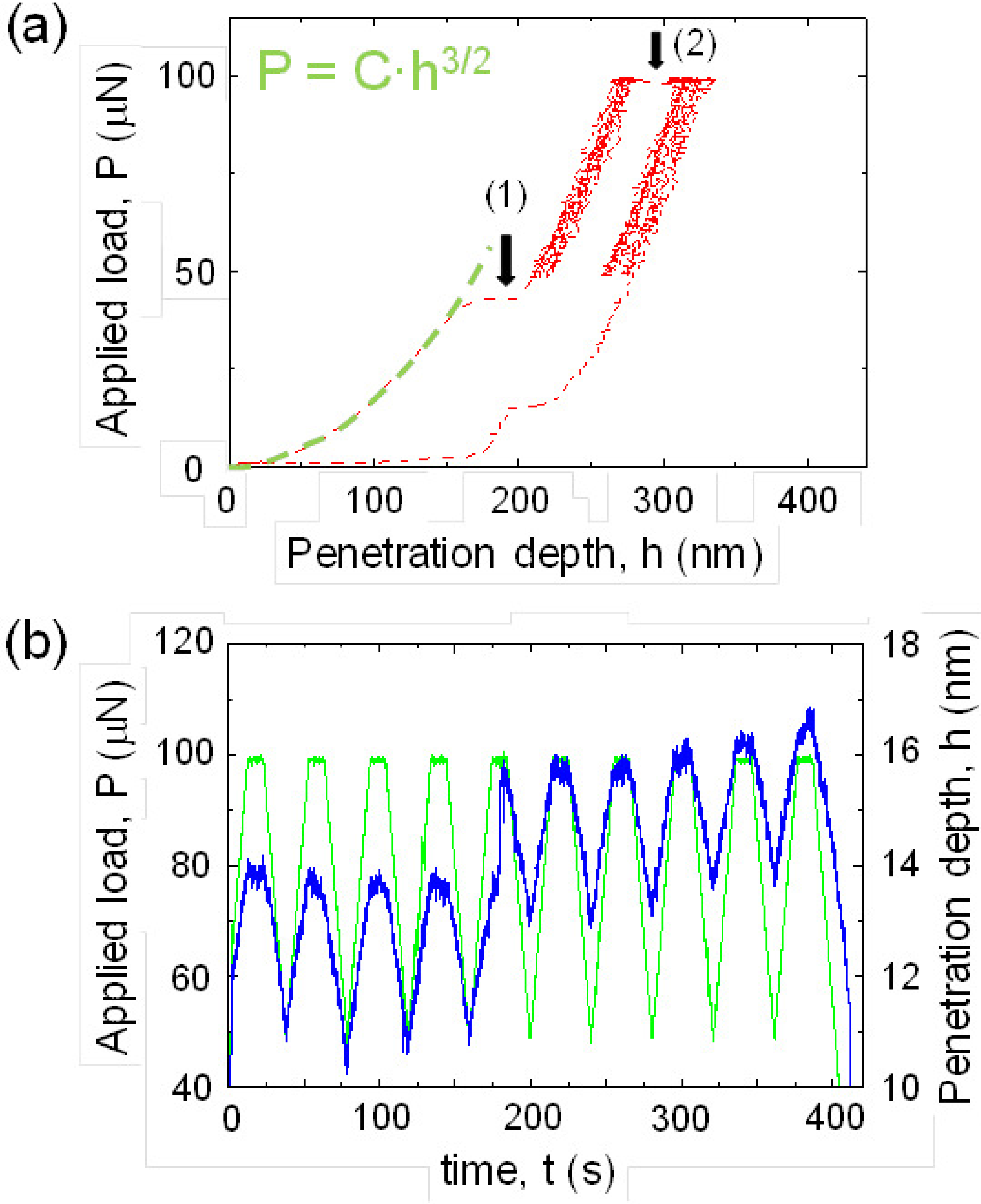
(a)
$P = C \cdot h^{3/2}$
(1)
(2)
Applied load, P (μN)
Penetration depth, h (nm)
(b)
Applied load, P (μN)
Penetration depth, h (nm)
time, t (s)

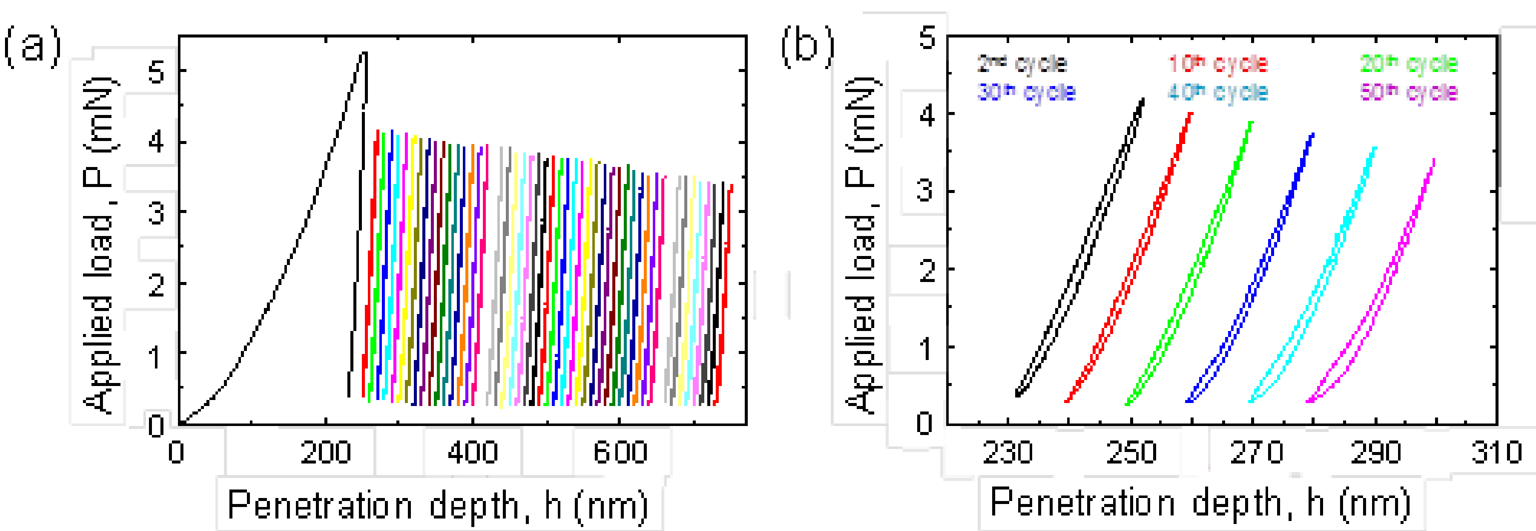
(a)
Applied load, P (mN)
0
1
2
3
4
5
0
200
400
600
Penetration depth, h (nm)
(b)
2nd cycle
10th cycle
20th cycle
30th cycle
40th cycle
50th cycle
Applied load, P (mN)
0
1
2
3
4
5
230
250
270
290
310
Penetration depth, h (nm)

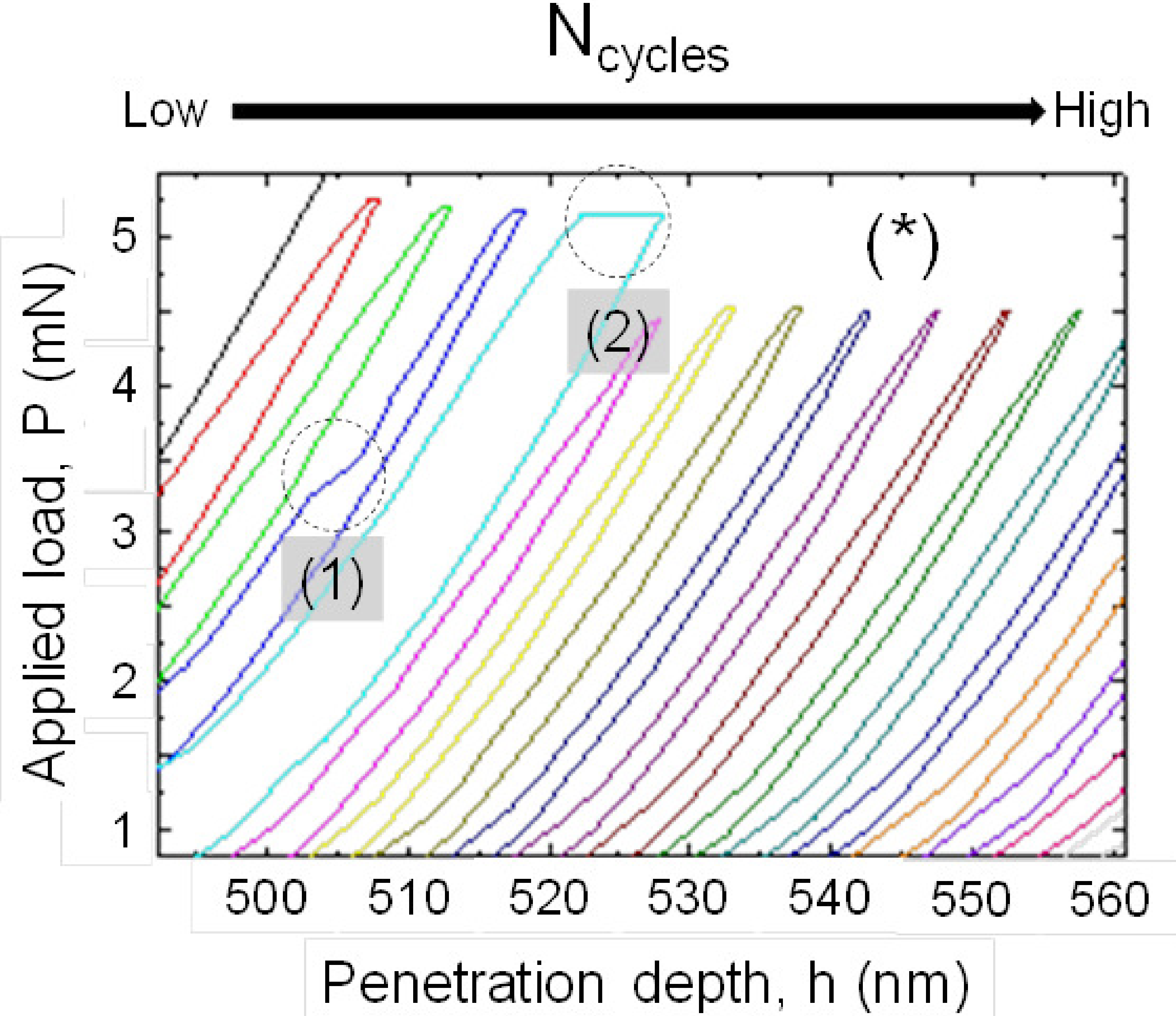

N cycles
Low
High
(*)
(2)
(1)
Applied load, P (mN)
5
4
3
2
1
500
510
520
530
540
550
560
Penetration depth, h (nm)

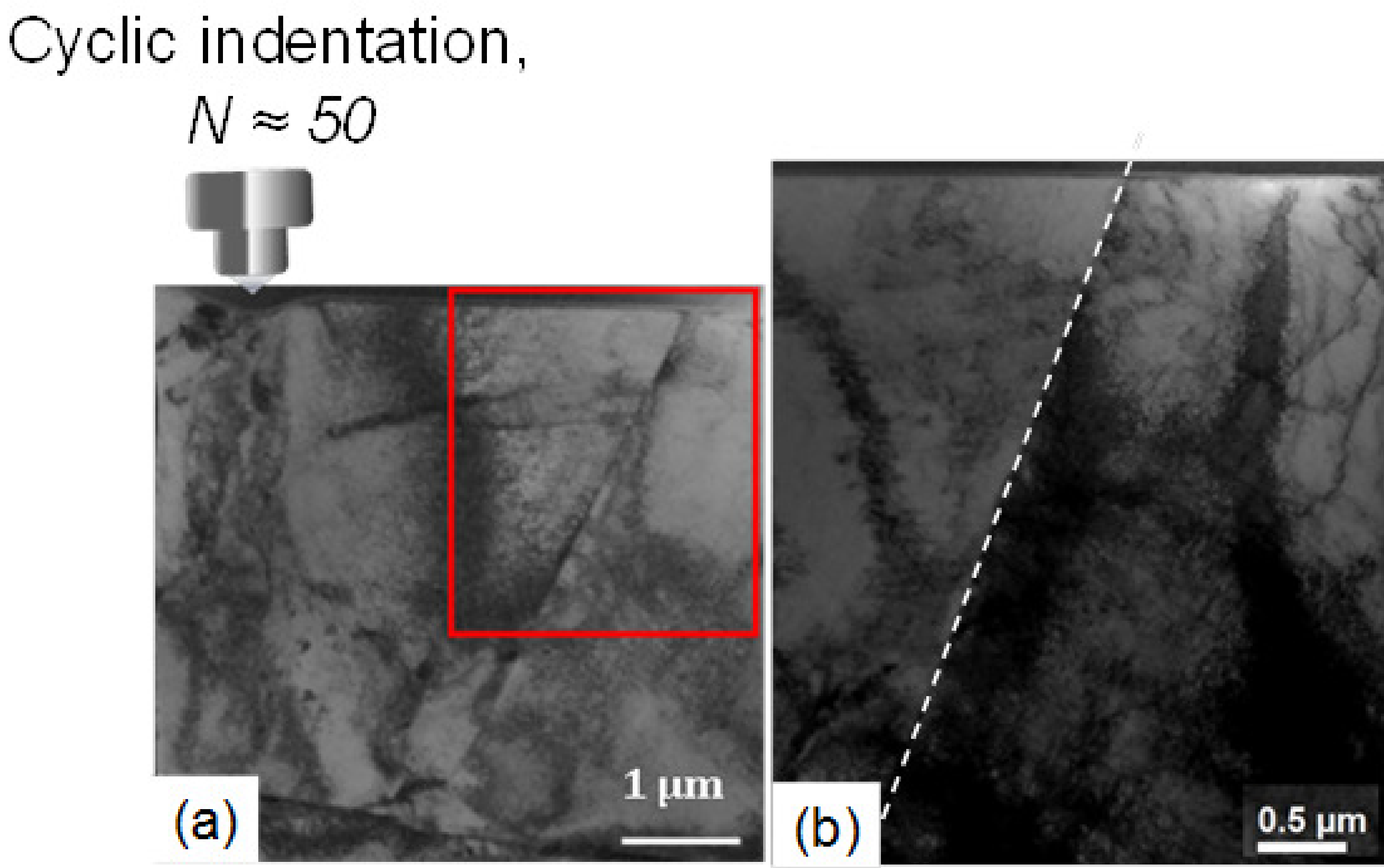
Cyclic indentation,
N ≈ 50
(a)
1 μm
(b)
0.5 μm

Table captions

Table 1. Chemical composition of the studied material (wt.%) obtained by microprobe for N and by SEM-EDX for the other elements.

Table 2. Summary of the tests inputs employed to conduct the different cyclic tests.

Table 1

C	Si	Mn	Cr	Ni	Cu	Mo	N	Fe
0.02	0.48	1.29	18.6	6.4	0.14	0.04	0.07	Bal.

Table 2

Working mode	Upper limit	Number of indentation cycles	Holding time (s)
Loading control	5 mN	2	0 and 10
		50	10